



## Short communication

## Quantum-well passivating contact at polysilicon/crystalline silicon interface for crystalline silicon solar cells

Duy Phong Pham <sup>a</sup>, Sungheon Kim <sup>b</sup>, Vinh-Ai Dao <sup>c,d</sup>, Youngkuk Kim <sup>a</sup>, Junsin Yi <sup>a,\*</sup><sup>a</sup> Department of Electrical and Computer Engineering, Sungkyunkwan University, Suwon 16419, Republic of Korea<sup>b</sup> Interdisciplinary Program in Photovoltaic System Engineering, Sungkyunkwan University, Suwon 16419, Republic of Korea<sup>c</sup> Future Materials & Devices Lab., Institute of Fundamental and Applied Sciences, Duy Tan University, Ho Chi Minh City 700000, Viet Nam<sup>d</sup> Faculty of Electrical-Electronic Engineering, Duy Tan University, Da Nang 550000, Viet Nam

## ARTICLE INFO

## ABSTRACT

## Keywords:

Passivating contact  
Silicon solar cells  
Quantum well  
Polysilicon contact

Polysilicon/crystalline silicon (poly-Si/c-Si) passivating contact is attracting attention as a promising passivation technology for c-Si solar cells. Recently, we have proposed a quantum-well passivating contact (QWPC) that uses a quantum-well at the poly-Si/c-Si interface to suppress recombination, such as Auger and/or Shockley-Read-Hall recombination, due to deep dopant-diffusion problems from poly-Si into the c-Si absorber and, as a result, promote the passivation quality. Herein, we demonstrate the effectiveness of the QWPC in a large area ( $272.13\text{ cm}^2$ ) of c-Si photovoltaic devices. A reference device, featuring a front boron diffusion emitter and normal rear poly-Si/c-Si passivating contact without QWPC, achieves a certified 22.99% conversion efficiency. The QWPC significantly reduces recombination losses within the device, as demonstrated by bias external quantum efficiency and dark I-V characteristics. The QWPC improves the open-circuit voltage ( $V_{oc}$ ) by 20 mV. An antireflection magnesium fluoride coating applied at the front along with the QWPC improves the short-circuit current density by  $1.27\text{ mA/cm}^2$ . The QWPC device achieves a conversion efficiency of 23.91%. The QWPC demonstrates an innovative passivating contact for promoting c-Si solar cell performance.

## 1. Introduction

The use of photovoltaic (PV) systems to convert solar energy into electricity is a feasible option for meeting rising global energy demand while minimising reliance on nonrenewable energy sources such as fossil fuels. The crystalline silicon (c-Si) solar cell has positioned itself as the market leader in photovoltaic devices due to its low cost and standardised commercial production technique. The objective of reducing commercial prices even further requires significant advancements in PV manufacturing technology and/or approaches to improve the efficiency of c-Si PV devices. In recent years, the silicon PV community has been attracted to the passivating-contact and/or carrier-selective contact (CSC) approaches for boosting c-Si solar cell efficiency [1–4]. Polysilicon-based passivating contacts (hereinafter poly-Si) have a high potential for high stability and exceptional passivation quality, resulting in more than 26% of laboratory-scale c-Si devices [5,6]. Some major drawbacks remain, including as the need to retain highly doped poly-Si for efficient additional field-effect passivation (AFP) while minimising extensively deep dopant diffusion into the c-Si

absorber during a high-temperature annealing step [7,8]. A shallow dopant in-diffusion to the host is necessary to provide the AFP. However, the excessive diffusion will cause significant recombination losses such as the Auger and/or Shockley-Read-Hall recombination, which degrades the open-circuit voltage ( $V_{oc}$ ) parameter. As a result, an in-diffusion trade-off is needed. It requires substantial optimisation of the thermal-annealing process as well as doping concentration. Technological advancement is critical for promoting passivation contact and, as a result, cell performance.

We recently reported on a quantum-well passivating contact (QWPC) that was inserted between the c-Si absorber and the poly-Si to improve passivation quality [9]. Massive dopant diffusion from the highly doped poly-Si into the absorber was efficiently restricted by the quantum well while retaining a tunnelling majority carrier transport. With a recombination current density ( $J_r$ ) of  $1.1\text{ fA/cm}^2$  and an implied open-circuit voltage ( $iV_{oc}$ ) of 742 mV, remarkable passivation quality was achieved. This work demonstrates the efficacy of the QWPC on the rear of a large-area tunnel oxide passivated contact (TOPCon) device with a front boron-diffused selective emitter and a phosphorous-doped poly-Si rear

\* Corresponding author.

E-mail addresses: [pdphong@skku.edu](mailto:pdphong@skku.edu) (D. Phong Pham), [junsin@skku.edu](mailto:junsin@skku.edu) (J. Yi).

contact. The QWPC passivation quality improved open-circuit voltage ( $V_{oc}$ ) by 20 mV. At the front, a magnesium fluoride ( $MgF_2$ ) antireflection coating was employed to enhance short-circuit current density ( $J_{sc}$ ), which enhanced  $J_{sc}$  by  $1.27 \text{ mA/cm}^2$ . As a result, the constructed QWPC-TOPCon device achieved a 23.91% efficiency, which was 0.92% higher than that of a certified reference TOPCon device. Measurements of dark I-V (DIV) and bias external quantum efficiency (EQE) are used to get insight into the efficacy of QWPC within the devices.

## 2. Experimental details

**Fig. 1a** and **1b** depict the schematic TOPCon structures of a reference device and a QWPC device, respectively, whereas **Fig. 1c** depicts the device's experimental progress. The devices were fabricated on an M6 (166-mm quasi-square) n-type Czochralski silicon wafer with resistivity ranging from 0.2 to 1  $\Omega\text{-cm}$ . After completing conventional Radio Corporation of America wet chemical treatments including alkaline texturing and surface cleaning, the wafers were doped to form a boron-doped emitter ( $p^+$ -emitter) in a boron diffusion furnace using  $BBr_3$  gas precursor. The boron-doped zone at the back was removed by a single-side etching using a mixture of hydrofluoric acid and nitric acid. The back surface was then thermally oxidised for 15 min at 700 °C to generate a 1.5-nm interfacial  $SiO_x$  layer. Following that, a highly phosphorous-doped hydrogenated amorphous silicon layer ( $n +$ -a-Si:H) and a stack of 5-nm a-Si:H/1.5-nm  $SiO_x/n +$ -a-Si:H were grown at the rear of the reference and QWPC devices, respectively, using a plasma-enhanced chemical vapour deposition (PECVD) system. After thermal annealing at 900 °C for 30 min in a rich-nitrogen environment, passivating contacts were formed at the back of the reference (**Fig. 1a**) and QWPC (**Fig. 1b**) devices. **Fig. 1b** depicts QWPC with a single quantum well inserted between the poly-Si layer and the c-Si wafer. A narrow-gap nanocrystalline silicon (nc-Si) layer confined between two wide-gap thin  $SiO_x$  layers defines the single quantum well. A passivation stack of  $AlO_x/SiN_x$  dielectric layers and a single  $SiN_x$  layer were formed on the front and back sides, respectively, after wet chemical etching and cleaning. Finally, the samples were screen-printed on both sides with grid-pattern 9-busbars, followed by a firing procedure at roughly 760 °C to entirely create metallization. Light I-V (LIV) curves and EQE were used to characterise the TOPCon devices after construction under conventional one-sun illumination (100 mW/cm<sup>2</sup>, AM1.5G, 25 °C). In a conventional dark room, dark I-V (DIV) curves were measured in a bias voltage range

from -1 V to 1 V.

## 3. Results and discussions

**Fig. 2a** shows the LIV data of the reference TOPCon device, which was measured independently at Fraunhofer ISE CalLab. **Fig. 2b** is a practical photograph of the TOPCon device. **Fig. 2c** and **2d** show LIV and EQE data of the devices. A reference-device efficiency was 22.99%, including an  $V_{oc}$  of 695.3 mV, a  $J_{sc}$  of 40.62  $\text{mA/cm}^2$ , and a fill factor (FF) of 81.4%. The  $V_{oc}$  of the reference device was deteriorated to be less than 700 mV.  $V_{oc}$  degradation was probable due to extensive dopant diffusion from the highly doped poly-Si into the c-Si absorber [7] at the rear, along with recombination losses due to direct contact between metal and the c-Si absorber at the front. Based on dopant diffusion profiles, as shown in **Fig. 3**, we found that the diffused dopant concentration of a sample with the quantum well was lower than that of the reference. The dopant concentration was below  $10^{19} \text{ cm}^{-3}$  at a distance of around 100 nm from the c-Si interface. The deep dopant diffusion caused a significant deterioration in AFP quality owing to insufficient isolation of the quasi-Fermi level, reducing band bending at the poly-Si/c-Si interface [7,9]. As a result, the hole may facilitate tunnelling over the barrier and recombine with electrons at the interface. Extensive dopant diffusion increased the  $J_o$  at the interface while decreasing the contact resistivity ( $\rho_c$ ) [9]. To minimise both  $J_o$  and  $\rho_c$ , it is critical to suppress deep dopant diffusion while maintaining a highly doped poly-Si degree for efficient AFP. **Fig. 4** shows cross-sectional high-resolution transmission electron microscopy (HRTEM) images of samples without (**Fig. 4a**) and with (**Fig. 4b**) the quantum well. The quantum-well structure with a nc-Si layer sandwiched between double  $SiO_x$  layers (~1.5 nm) at the poly-Si/c-Si interface, as shown in **Fig. 4b**, restricts diffusion due to the double  $SiO_x$  diffusion barrier, which can impede diffusion to a greater extent than the reference device's single  $SiO_x$  barrier (**Fig. 4a**) [9]. **Fig. 5a** and **5b** illustrate band diagrams for carrier collection at the rear of the reference and QWPC devices, respectively. It indicates that the nc-Si layer can serve as an intermediate conductive channel for carriers tunnelling through double thin  $SiO_x$  layers toward the collection. The optimal conditions and QWPC mechanism have been reported elsewhere [9]. As a result, as shown in **Fig. 2c**, the QWPC device achieved a  $V_{oc}$  of 715.3 mV, which was 20 mV higher than that of the reference. As shown in **Fig. 2d**, the addition of a  $MgF_2$  layer decreased reflectance losses at the front and raised the EQE of the QWPC

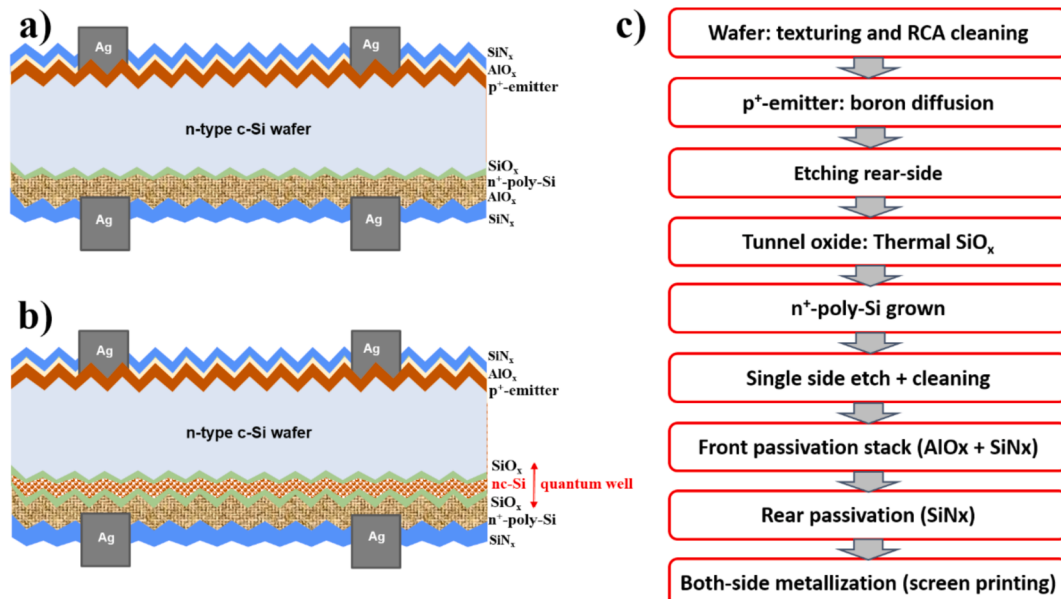


**Fig. 1.** Schematic diagram structures of the reference TOPCon device (a) and the QWPC device (b), and experimental procedure of the device (c).

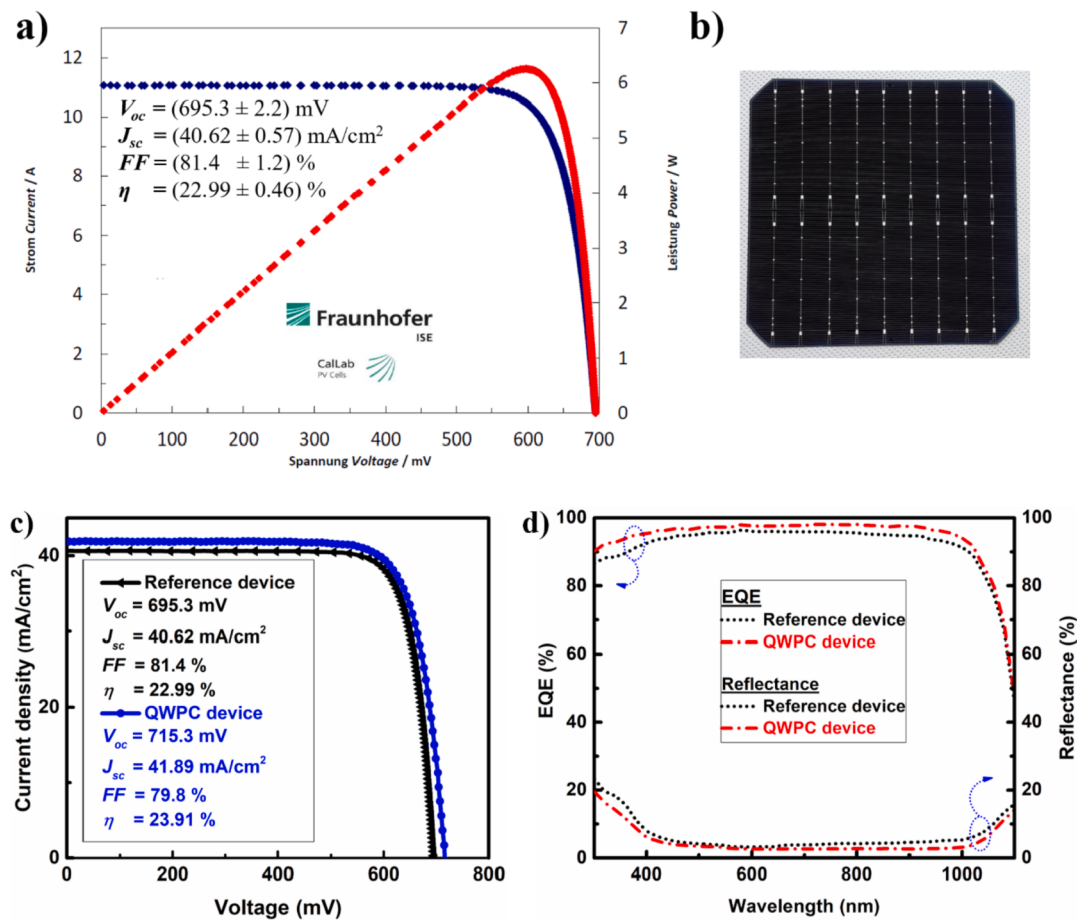


**Fig. 2.** (a) LIV data of the reference device measured at Fraunhofer ISE CalLab, (b) real photo of the device at the front side, (c) LIV data, and (d) EQE data of the devices.

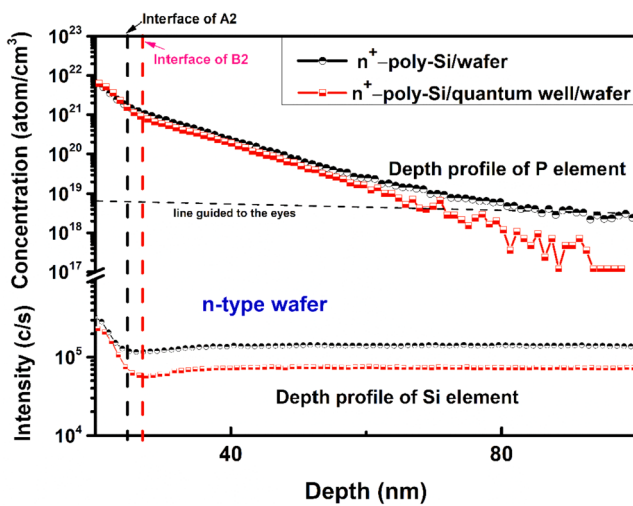


**Fig. 3.** SIMS profiles of poly-Si passivating contacts with and without the quantum well at the poly-Si/c-Si wafer interface. Reused with permission from reference [9].

device, as compared to that of the reference. As a result, the  $J_{sc}$  of the QWPC device was  $41.89$  mA/cm $^2$ , which was about  $1.27$  mA/cm $^2$  higher than the reference. Based on the increases in  $V_{oc}$  and  $J_{sc}$ , the QWPC device had a conversion performance of  $23.91\%$ , which was  $0.92\%$  greater than the reference device.

To get insight into the quantum-well effect, the bias EQE approach

was used on the devices. When a forward bias is applied to the device, which provides positive and negative voltages to the p-type doped and n-type doped sections, respectively, the internal electric field inside the device reduces significantly, restraining carrier transport to their collecting electrodes. In this case, the carrier transport is mostly hindered by recombination losses inside the device. A substantial decrease in the forward-bias EQE may indicate severe recombination losses inside the device. As a consequence, a forward-bias EQE ratio (EQE (0.5 V)/EQE (0 V)) less than one might reflect the degree of recombination inside a device [10,11]. A reverse bias, on the other hand, increases the internal electric field, which promotes carrier transport to their collecting electrodes. A significant increase in reverse-bias EQE may indicate a high level of recombination or defects inside a device. It means that providing the internal electric field of reverse-bias is expected to transport carriers massively over defect-traps within a device to their collecting electrodes. As a consequence, a considerable increase in the reverse-bias EQE ratio (EQE (-0.5 V)/EQE (0 V)) inside a device may indicate a high degree of recombination [12]. The forward- and reverse-bias EQE ratios of the devices are shown in Fig. 6a and 6b, respectively. The bias EQE measurements were performed on the QWPC device without the MgF $_2$  layer at the front for a more precise comparison. The QWPC device has a higher forward-bias EQE ratio than the reference, notably at long wavelengths (above 800 nm), which are absorbed mostly towards the back. It indicated that the QWPC device exhibited lower recombination and/or carrier collection losses than the reference device, particularly at the back. This was due to the quantum well significantly decreasing dopant diffusion into the c-Si absorber, hence enhancing the passivation quality at the back. In the wavelength range, the quantum-well device's reverse-bias EQE ratio was lower than that of the reference, as shown in

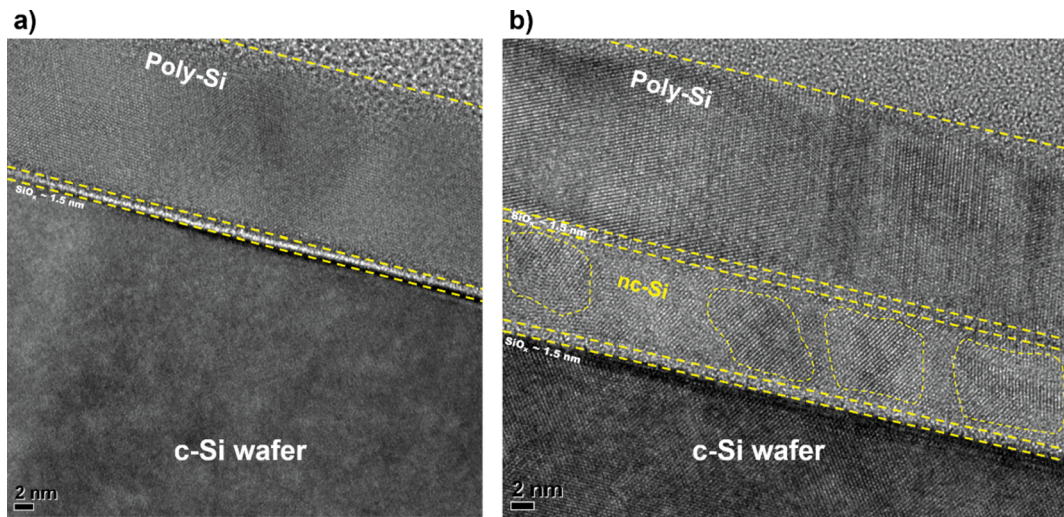


**Fig. 4.** Cross-sectional HRTEM images of poly-Si passivating contacts a) without and b) with the quantum well at the poly-Si/c-Si interface.

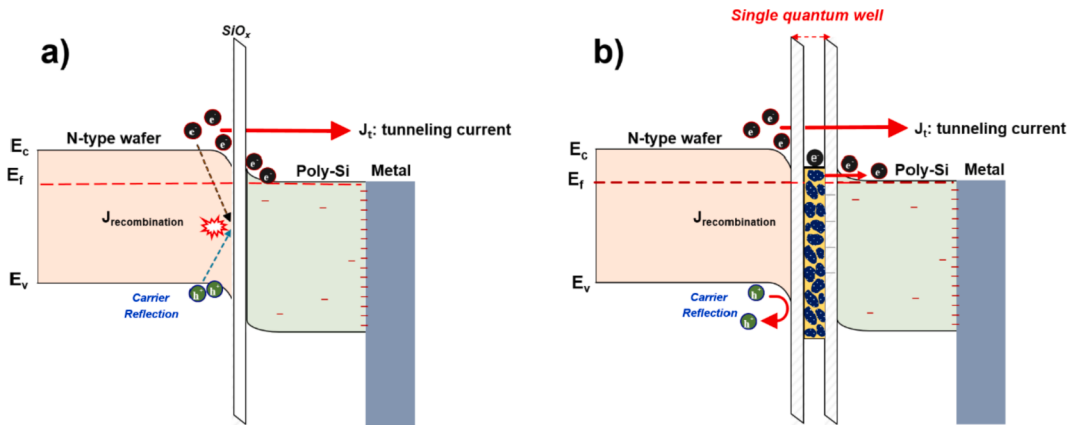


**Fig. 5.** Band diagram for carrier collection at the rear of a) the reference and b) QWPC devices.

**Fig. 6b.** It proved that, when compared to the reference, the QWPC device minimised recombination losses within the device. Because the front structure of both devices was made the same way, recombination losses were thought to be concentrated on the back side because of dopant diffusion.

To clarify the recombination losses further, DIV was studied as illustrated in Fig. 7. In DIV, the injected carrier concentration is mostly determined by the bias voltage applied, whereas recombination caused by defects within a device has an effect on the carrier concentration and/or transportation. As a result, different current responses to various bias voltages may give additional information regarding recombination. The following equation expresses the relationship between dark current density ( $J$ ) and bias voltage ( $V$ ) in the device's dark state:

$$J = J_0[\exp(q(V - J.R_s)/nkT) - 1] - [(V - J.R_s)/R_{sh}] \quad (1)$$

where  $q$  denotes the elementary charge,  $k$  the Boltzman constant,  $J_0$  the reverse saturation current density,  $n$  the ideality diode factor,  $T$  the absolute temperature,  $R_s$  the series resistance, and  $R_{sh}$  the shunt resistance.

Because  $R_{sh}$  is significantly greater than  $R_s$ , the second component of the equation could be insignificant to the calculation and may therefore be removed. The derivative  $dV/dJ$  is represented as follows from the resultant equation (1):

$$dV/dJ = R_s + [(nkT/q)/J] \quad (2)$$

**Fig. 7a** depicts plots of  $dV/dJ$  as a function of  $1/J$  in the high bias region ( $V \geq 0.6$  V). In this region, the dark current is mainly determined by the  $R_s$  variation [13,14]. Using equation (2),  $R_s$  values are derived from the intercepts of the plots. **Fig. 7b** shows the plotting  $\log(J)$  as a function of  $(V - JR_s)$  using the  $R_s$  values derived from (2). Linear fittings of the plots (Fig. 7b) produce slope  $q/nkT$  and an intercept  $J_0$ . The  $R_s$ ,  $n$ , and  $J_0$  values of the devices are tabulated in the insets of Fig. 7a and 7b.

Because the quantum well can suppress deep dopant diffusion, increasing contact resistance [9], the  $R_s$  of the QWPC device was slightly higher than that of the reference. As a result, the FF of the QWPC device was slightly lower than that of the reference, as shown in Fig. 2. The reference device's  $n$  value was closer to 2, indicating that the recombination current dominated the device's conduction mechanism [15]. The recombination could be caused mainly by deep dopant diffusion from the poly-Si into the absorber. The  $n$  value of the QWPC device, on the other hand, was closer to unity, indicating that the diffusion current seems to dominate inside the device [16]. Furthermore, the QWPC device's  $J_0$  was much lower than that of the reference. This means that the quantum-well device significantly decreases recombination losses inside the device. Deep dopant diffusion may be responsible for the change of the conduction mechanism from recombination of the reference device to the diffusion current mechanism of the quantum-well device. Diffusion might produce considerable recombination along the poly-Si/c-Si interface, increasing the  $n$  and  $J_0$  parameters of the reference device. The recombination current model in the dark condition is vitally defined

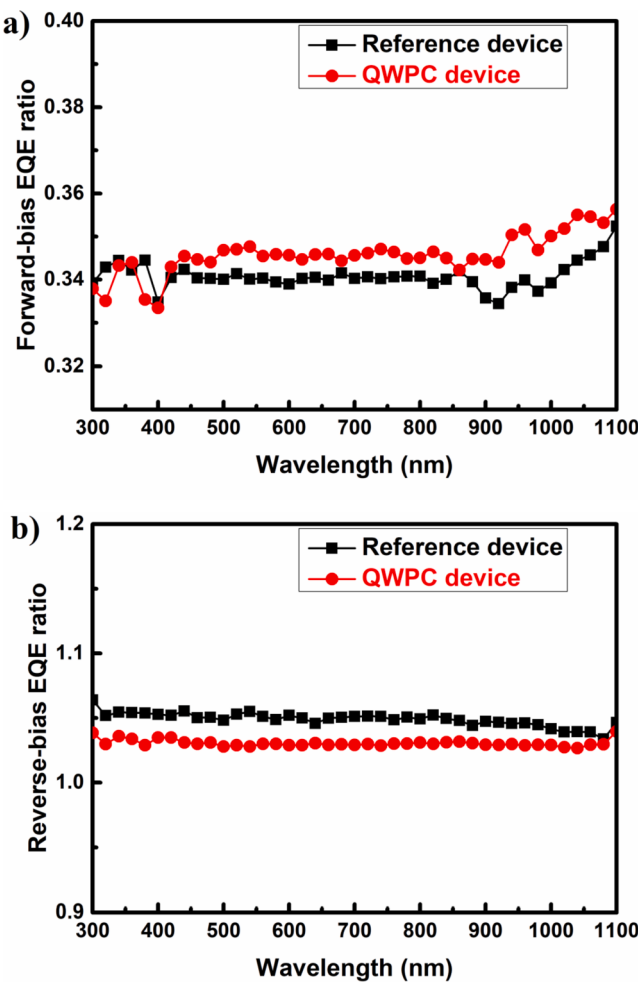


Fig. 6. a) Forward bias and b) reverse bias EQE ratios of the devices.

at the depletion zone and/or the space charge region in an ideal p-n junction model. However, in a real device, the recombination model seems to be more complicated owing to the existence of various additional components, such as surface recombination and/or other semiconductor/metal contacts, which may have a major influence on  $n$  and  $J_0$ . Some researchers believe that the recombination model is susceptible to interfacial defects or recombination [17,18]. As a result, the change in the conduction mechanism may be explained by lowering the recombination losses caused by the quantum-well at the poly-Si/c-Si interface.

#### 4. Conclusion

The effectiveness of QWPC at the poly-Si/c-Si interface was demonstrated in the large-area TOPCon devices. The purpose of the QWPC was to suppress the massive dopant diffusion from the poly-Si into the c-Si due to the double  $\text{SiO}_x$  barriers, resulting in improved passivation quality and, as a result,  $V_{\text{oc}}$ . The QWPC device showed a 20 mV higher  $V_{\text{oc}}$  than the reference. The bias EQE technique demonstrated that the QWPC device significantly reduced the recombination losses within the device, especially at the rear region of the device, compared with the reference. The DIV results demonstrated that the conductivity mechanism changed from the recombination of the reference device into the diffusion currents of the QWPC device. Furthermore,  $n$  factors suggested that surface recombination was primary in the reference device's recombination losses. As a result, the QWPC was an innovative technique to suppress the recombination losses at the surface of TOPCon devices.

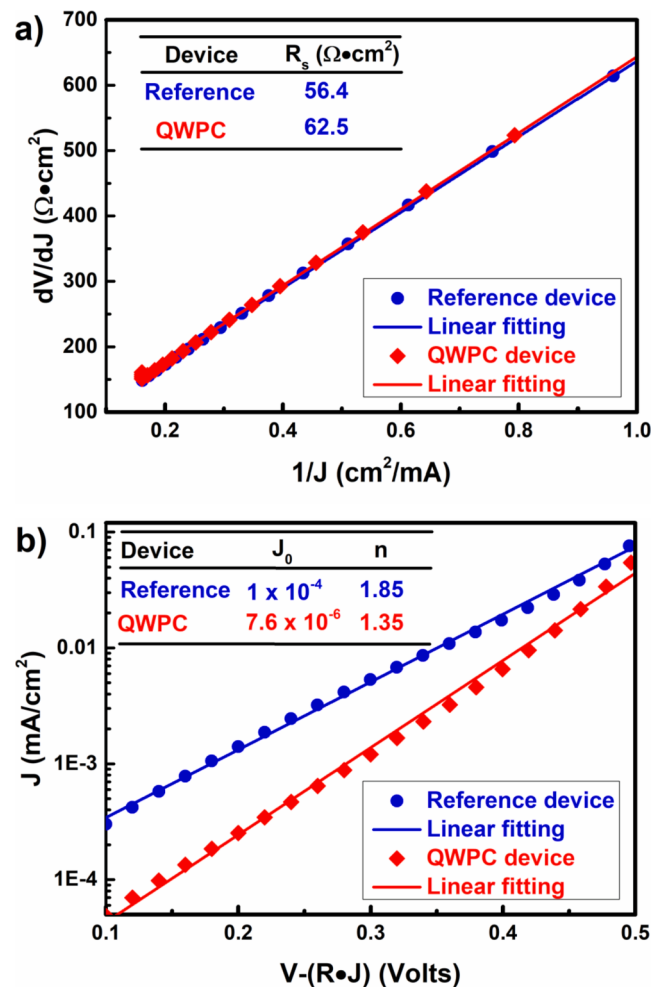


Fig. 7. (a)  $dV/dJ$  as a function of  $1/J$ .  $R_s$  values, extracted from intercept of the linear fittings, are tabulated in the inset. (b)  $\log(J)$  as a function of  $(V - J \cdot R_s)$ .  $J_0$  and  $n$  values, extracted from intercepts and slopes of the linear fittings, respectively, are tabulated in the inset.

#### Funding

This work was supported by the Korea Institute of Energy Technology Evaluation and Planning (KETEP) grant funded by the Korea government (MOTIE) (No. 20213030010400) and (No. 20203040010320).

#### Declaration of Competing Interest

The authors declare that they have no known competing financial interests or personal relationships that could have appeared to influence the work reported in this paper.

#### Data availability

Data will be made available on request.

#### References

- [1] T.G. Allen, J. Bullock, X. Yang, A. Javey, S. De Wolf, Passivating contacts for crystalline silicon solar cells, *Nat. Energy* 4 (11) (2019) 914–928.
- [2] S. Chander, A. Purohit, A. Sharma, S.P. Arvind, M.S.D. Nehra, A study on photovoltaic parameters of mono-crystalline silicon solar cell with cell temperature, *Energy Rep.* 1 (2015) 104–109.
- [3] G. Yang, A. Ingenito, O. Isabella, M. Zeman, IBC c-Si solar cells based on ion-implanted poly-silicon passivating contacts, *Sol. Energy Mater. Sol. Cells* 158 (2016) 84–90.

- [4] S. Chander, A. Purohit, A. Sharma, S.P. Nehra, M.S. Dhaka, Impact of temperature on performance of series and parallel connected mono-crystalline silicon solar cells, *Energy Rep.* 1 (2015) 175–180.
- [5] F. Haase, C. Hollemann, S. Schäfer, A. Merkle, M. Rienäcker, J. Krügener, R. Brendel, R. Peibst, Laser contact openings for local poly-Si-metal contacts enabling 26.1%-efficient POLO-IBC solar cells, *Sol. Energy Mater. Sol. Cells* 186 (2018) 184–193.
- [6] F. Feldmann, M. Bivour, C. Reichel, M. Hermle, S.W. Glunz, Passivated rear contacts for high-efficiency n-type Si solar cells providing high interface passivation quality and excellent transport characteristics, *Sol. Energy Mater. Sol. Cells* 120 (2014) 270–274.
- [7] D.P. Pham, J. Yi, Dopant-grading proposal for polysilicon passivating contact in crystalline silicon solar cells, *J. Power Sources* 522 (2022), 231005.
- [8] A. Ingenito, G. Nogay, Q. Jeangros, E. Rucavado, C. Allezé, S. Eswara, N. Valle, T. Wirtz, J. Horzel, T. Koida, M. Morales-Masis, M. Despeisse, F.-J. Haug, P. Löper, C. Ballif, A passivating contact for silicon solar cells formed during a single firing thermal annealing, *Nat. Energy* 3 (9) (2018) 800–808.
- [9] D.P. Pham, S. Lee, M. Quddamah Khokhar, S. Chowdhury, H. Park, Y. Kim, E.-C. Cho, J. Yi, Innovative passivating contact using quantum well at poly-Si/c-Si interface for crystalline silicon solar cells, *Chem. Eng. J.* 423 (2021), 130239.
- [10] D.P. Pham, S. Kim, J. Park, A.H. Tuan Le, J. Cho, J. Jung, S.M. Iftiquar, J. Yi, Reduction in Photocurrent Loss and Improvement in Performance of Single Junction Solar Cell Due to Multistep Grading of Hydrogenated Amorphous Silicon Germanium Active Layer, *Silicon* 10 (3) (2017) 759–767.
- [11] D.P. Pham, S. Kim, J. Park, A.H.T. Le, J. Cho, J. Yi, Improvement in carrier collection at the i/n interface of graded narrow-gap hydrogenated amorphous silicon germanium solar cells, *J. Alloy. Compd.* 724 (2017) 400–405.
- [12] D.P. Pham, S. Kim, J. Park, A.T. Le, J. Cho, J. Jung, S.M. Iftiquar, J. Yi, Silicon germanium active layer with graded band gap and μc-Si: H buffer layer for high efficiency thin film solar cells, *Mater. Sci. Semicond. Process.* 56 (2016) 183–188.
- [13] R. Hussein, D. Borchert, G. Grabosch, W.R. Fahrner, Dark I-V-T measurements and characteristics of (n) a-Si/pc-Si heterojunction solar cells, *Sol. Energy Mater. Sol. Cells* 69 (2001) 123–129.
- [14] V.-A. Dao, T.T. Trinh, S. Kim, L. Van Ngoc, T.D. Viet, N.T. Thanh Giang, D. L. Duong, H.T. Thanh Nguyen, N.D. Nam, J. Yi, J. Kim, Carrier transport mechanisms of reactively direct current magnetron sputtered tungsten oxide/n-type crystalline silicon heterojunction, *J. Power Sources* 472 (2020), 228460.
- [15] S. Kim, J. Lee, V.A. Dao, S. Lee, N. Balaji, S. Ahn, S.Q. Hussain, S. Han, J. Jung, J. Jang, Y. Lee, J. Yi, Effects of LiF/Al back electrode on the amorphous/crystalline silicon heterojunction solar cells, *Mater. Sci. Eng., B* 178 (9) (2013) 660–664.
- [16] S. Kim, J. Jung, Y.-J. Lee, S. Ahn, S.Q. Hussain, J. Park, B.-S. Song, S. Han, V. A. Dao, J. Lee, J. Yi, Role of double ITO/In2O3 layer for high efficiency amorphous/crystalline silicon heterojunction solar cells, *Mater. Res. Bull.* 58 (2014) 83–87.
- [17] Y. Lee, V.A. Dao, S.M. Iftiquar, S. Kim, J. Yi, Current transport studies of amorphous n/p junctions and its application in a-Si:H/HIT-type tandem cells, *Prog. Photovoltaics Res. Appl.* 24 (1) (2016) 52–58.
- [18] D.P. Pham, S. Kim, J. Park, J. Cho, H. Kim, A.H.T. Le, J. Yi, Role of a-Si: H buffer layer at the p/i interface and band gap profiling of the absorption layer on enhancing cell parameters in hydrogenated amorphous silicon germanium solar cells, *Optik* 136 (2017) 507–512.